JOURNAL OF THERMOPHYSICS AND HEAT TRANSFER
Vol. 19, No. 1, January–March 2005

Semiconductor Crystal Growth by Modified Vertical Gradient Freezing with Electromagnetic Stirring

Xianghong Wang* and Nancy Ma†
North Carolina State University, Raleigh, North Carolina 27695
and
David F. Bliss‡ and Gerald W. Iseler‡
U.S. Air Force Research Laboratory, Hanscom Air Force Base, Massachusetts 01731

This paper presents a numerical model for the unsteady transport of a dopant during the VGF process by submerged heater growth with a steady axial magnetic field and a steady radial electric current. Electromagnetic (EM) stirring can be induced in the gallium-antimonide melt just above the crystal growth interface by applying a small radial electric current in the melt together with an axial magnetic field. The application of EM stirring provides a significant convective dopant transport in the melt so that the crystal solidifies with relatively good radial and axial homogeneity. Dopant distributions in the crystal and in the melt at several different stages during growth are presented.

I. Introduction

GALLIUM ANTIMONIDE (GaSb) bulk semiconductor crystals with high optical transmission are extremely important for space-based imaging applications. These crystals are typically doped with an element such as selenium, which gives the crystal the needed optical and electrical properties. The performance of a semiconductor is directly proportional to the uniformity of its dopant composition so it is crucial that the crystal has as little segregation as possible. Investigations for the melt growth of uniformly-doped gallium-antimonide (GaSb) semiconductor crystals as well as other III-V alloy crystals with uniform composition, are underway at the U.S. Air Force Research Laboratory at Hanscom Air Force Base by the vertical gradient freeze (VGF) method utilizing a submerged heater. Bulk gallium antimonide crystals can be grown from the melt by the liquid-encapsulated Czochralski (LEC) process or by the vertical-gradient freeze (VGF) process. The LEC process is a top-seeded growth method that has distinct advantages, because the crystal is viewed directly during growth and because there is no container in contact with the crystal. However, short-range compositional uniformity can be problematic due to buoyancy-driven convection in the melt, which randomly changes the composition of the melt in the boundary layer at the growth interface.[1] In addition, long-range crystal composition generally changes due to changing melt composition for dopants or alloys with segregation coefficients not equal to unity. Relatively good long-range compositional uniformity was achieved by the LEC process for a nonstoichiometric Sb-rich melt by Ohmori et al.[2] However, only 25% of the melt volume was solidified because the continual increase of antimony in the melt as crystal growth progressed eventually caused the crystal–melt interface to break down due to constitutional supercooling. In the early 90s, Ostrogorsky[3] introduced a modification of the bottom-seeded VGF process in which a submerged heater separates the melt into two zones, namely, a lower melt and an upper melt. As crystal growth progresses, the crystal solidifies and the submerged heater is slowly raised to maintain a constant lower melt depth. The lower melt is continuously replenished with liquid from the upper melt with a composition chosen to offset the increasing dopant level in the lower melt due to rejection at the crystal growth front for dopants with segregation coefficients less than unity. Unfortunately, there can be severe long-range axial segregation in the crystal if the process does not have a way to replenish the melt with a composition that offsets rejection of species along the crystal–melt interface.[4] Ostrogorsky[3] have shown that this modified bottom-seeded VGF method produces crystals that exhibit much lower defect densities and much more dopant uniformity than crystals grown by the LEC process.

Because molten gallium antimonide is a good electrical conductor, a radial electric current in the melt can be used together with an axial magnetic field to stir the melt in order to control the dopant distribution in the semiconductor crystal, which depends on the convective and diffusive transport of the dopant in the melt. We have demonstrated that a radial electric current of a few amperes in the presence of a 40-G axial magnetic field can produce stirring rates of up to 20 rpm in a gallium antimonide melt having diameter 50 mm and depth 1 cm. Some of the advantages of electromagnetic (EM) stirring for bottom-seeded crystal growth are enhancement of radial dopant uniformity, reduction of thermal stresses, minimization of defect densities, and the ability to grow at higher rates.

The large number of adjustable crystal-growth parameters and the larger number of ways to combine them make process optimization through trial and error extremely tedious. The strength of the magnetic field and electric current in the melt, for example, determine the stirring rate, but the current may also create Joule heating or Peltier cooling or heating. In addition, the relative heatfluxes from the various heaters compared to those from the submerged heater influence the shape of the crystal–melt interface. Therefore, models that predict dopant or alloy distribution in the melt together with heat transfer would be very useful for optimizing the complex growth process in a timely fashion. In a previous study,[5] we presented a transient model that treats the species transport of selenium (Se) in a gallium antimonide melt during the VGF process using a submerged heater and with a uniform, steady axial magnetic field and a steady radial electric current and found that the homogeneity improves as the strength of the electromagnetic stirring increases. In the present paper, we investigate the effect of much stronger electromagnetic stirring on the dopant segregation in the melt and in the crystal.

II. Melt Motion

This paper treats the unsteady, axisymmetric transport of selenium in a gallium antimonide melt during vertical-gradient-freeze

Received 20 April 2004; accepted for publication 9 June 2004; presented as Paper 2005-0916 at the AIAA 43rd Aerospace Sciences Meeting and Exhibit, Reno, NV, 10–13 January 2005.

*Graduate Research Assistant, Department of Mechanical and Aerospace Engineering, Campus Box 7910.
†Assistant Professor, Department of Mechanical and Aerospace Engineering, Campus Box 7910; nancy_ma@ncsu.edu. Senior Member AIAA.
‡Physicist, Sensors Directorate, AFRL/SNHC, 80 Scott Road.

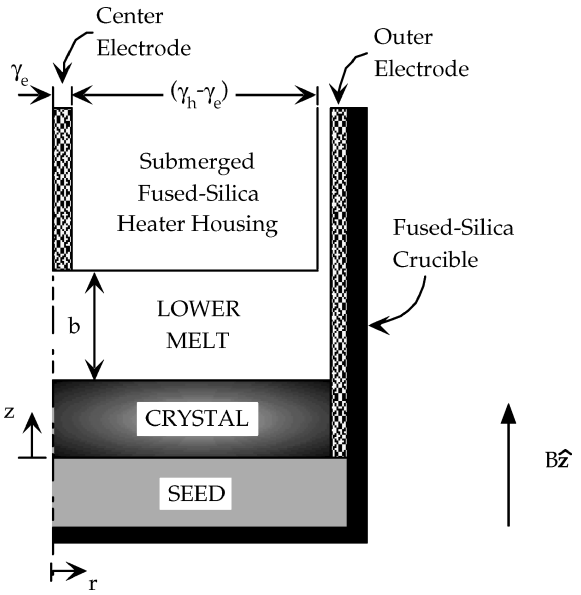

Fig. 1 VGF process using submerged heater growth with a uniform, steady, axial magnetic field $B\hat{z}$ and with a steady radial electric current where coordinates are normalized by the outer electrode's inner radius.

crystal growth using a submerged heater with an externally applied uniform, steady axial magnetic field $B\hat{z}$ combined with a radial electric current. Here, B is the magnetic flux density, whereas $\hat{r}$, $\hat{\theta}$, and $\hat{z}$ are the unit vectors for the cylindrical coordinate system. Our dimensionless problem is sketched in Fig. 1. The coordinates and lengths are normalized by the outer electrode's inner radius R, which is equal to the crystal radius, so that γ_e is the dimensionless radius of the center electrode, γ_h is the dimensionless radius of the submerged fused-silica heater housing, and b is the dimensionless depth of the lower melt. The electrodes are made of AXF-5Q graphite, which is manufactured by Poco Graphite. This graphite has an electrical conductivity equal to 1.47×10^{11} S/m. A single crystal seed, which initiates solidification, lies at the bottom of the fused-silica crucible. A graphite disc and a boron nitride disc lie below the crucible. These discs are cooled by a water-cooled hearth which removes heat along the bottom of the crucible. The submerged heater above the lower melt and the heaters adjacent to the periphery of the crucible are adjusted so that the crystal-melt interface is nearly planar, and the melt adjacent to the submerged heater is held at a uniform and constant temperature T_h. As the crystal at $z = \omega t$ solidifies, the crystal–melt interface moves axially upward at the dimensionless rate $\omega = U_g/U_c$, where U_g is the constant growth rate and U_c is the characteristic velocity of the melt, whereas z is normalized by the crystal's radius R and t is time normalized by R/U_c. The lower melt is replenished with liquid supplied from an upper melt to a small annular gap between the submerged heater and the outer electrode. The submerged heater at $z = \omega t + b$ moves upward at the same rate, so that the depth of the melt is constant throughout growth. A long cylindrical graphite electrode at the centerline moves with the submerged heater and carries a constant axially downward dc electric current. The electrical conductivity of the graphite electrodes is much larger than that of either the molten semiconductor, the fused-silica heater housing, or the crystal, so that the electric current chooses to travel through the long outer graphite electrode tube that rests inside the periphery of the crucible.

A magnetic field is applied with a copper coil outside the heater insulation, while an electric current is applied through the electrode so that the electromagnetic (EM) body force created by this electric current is balanced by the inertial force. This balance gives a characteristic velocity,

$$U_c = (BJ_cR/\rho_0)^{\frac{1}{2}} \tag{1}$$

where R is the inner radius of the outer electrode or the radius of the crystal, and ρ_0 is the density of the molten semiconductor at the melting temperature T_m. Here, the characteristic electric-current density is $J_c = I/(2\pi r_0 bR)$, where r_0 is a radial position that can be used to provide an approximate estimate of the radial electric current density. For crystal grown with $R = 25$ mm, $b = 0.4$, and $r_0 = 1$ cm, and for electromagnetic stirring produced with $I = 4$ A, our estimate of J_c is 6366.2 A/m^2 and the characteristic velocity is $U_c = 0.01027$ m/s. The thermophysical properties of gallium antimonide[6,7] are provided in Table 1.

Table 1 Thermophysical properties for molten GaSb

Property	Value
Density ρ_0, kg/m^3	6030
Dynamic viscosity μ, Pa · s	0.00231
Thermal conductivity k, W/m · K	17.1
Specific heat c_p, J/kg · K	328
Electrical conductivity σ, S/m	1×10^6
Thermal coefficient of volumetric expansion β_T, K^{-1}	0.0000958

The electric current in the melt produces an induced magnetic field that is superimposed upon the applied magnetic field produced by the external magnet. The characteristic ratio of the induced to applied magnetic field strengths is the magnetic Reynolds number, $R_m = \mu_p \sigma U_c R$, where μ_p is the magnetic permeability of the melt and σ is the electrical conductivity of the melt. For all crystal-growth processes, $R_m \ll 1$, and the additional magnetic fields produced by the electric currents in the melt are negligible.

Ohm's law is

$$\boldsymbol{j} = -\nabla\phi + N\boldsymbol{v} \times \hat{\boldsymbol{z}} \tag{2}$$

where j is the electric current density normalized by J_c, ϕ is the electric potential normalized by $J_c R/\sigma$, and $\boldsymbol{v} = v_r\hat{\boldsymbol{r}} + v_\theta\hat{\theta} + v_z\hat{\boldsymbol{z}}$ is the melt velocity normalized by U_c. Here, the ratio of the induced electric field $\boldsymbol{v} \times \hat{\boldsymbol{z}}$ to the static electric field $\nabla\phi$ is the interaction parameter $N = \sigma B^2 R/\rho_0 U_c$. For the present process with $B = 0.004$ T and $I = 4$ A, $N = 0.006$, so that the induced electric field is negligible. For our axisymmetric problem, there is no azimuthal flow of electric current, and the electric potential is governed by

$$\nabla^2\phi = 0 \tag{3}$$

We treat the electrodes as perfect conductors that carry a uniform electric potential. The boundary conditions are

$$\phi = 0, \quad \text{at} \quad r = 1, \quad \text{for} \quad -1 \le \zeta \le +1 \tag{4a}$$

$$\phi = \Phi_0, \quad \text{at} \quad \zeta = +1, \quad \text{for} \quad 0 \le r \le \gamma_e \tag{4b}$$

Here, $\zeta = -1 + 2(z - \omega t)/b$ is a rescaled axial coordinate such that $-1 \le \zeta \le +1$. The fused-silica heater, the annular gap between the heater and the outer electrode, and the crystal–melt interface are treated as electrical insulators so that $\hat{\boldsymbol{n}} \cdot \nabla\phi = 0$, where $\hat{\boldsymbol{n}}$ is the outward unit normal vector. The electric potential is given by a separation-of-variables solution,

$$\phi = \sum_{n=0}^{\infty} A_n \Phi_0 J_0(\lambda_n r) \frac{\cosh[(\lambda_n b/2)(\zeta + 1)]}{\cosh(\lambda_n b)} \tag{5}$$

where J_0 is the Bessel function of the first kind and zeroth order and λ_n are the eigenvalues of J_0. Based on our choice for the characteristic electric current density J_c, the integral of the radial electric current over the melt depth must equal b at $r = r_0$, so that

$$\Phi_0 = b\left[\sum_{n=1}^{\infty} A_n J_1(\lambda_n r_0) \frac{\sinh(\lambda_n b)}{\cosh(\lambda_n b)}\right]^{-1} \tag{6}$$

where J_1 is the Bessel function of the first kind and first order. A Galerkin method is implemented to avoid a Gibbs phenomenon associated with the discontinuous boundary conditions along $\zeta = +1$. The electric current originates from the center electrode and flows

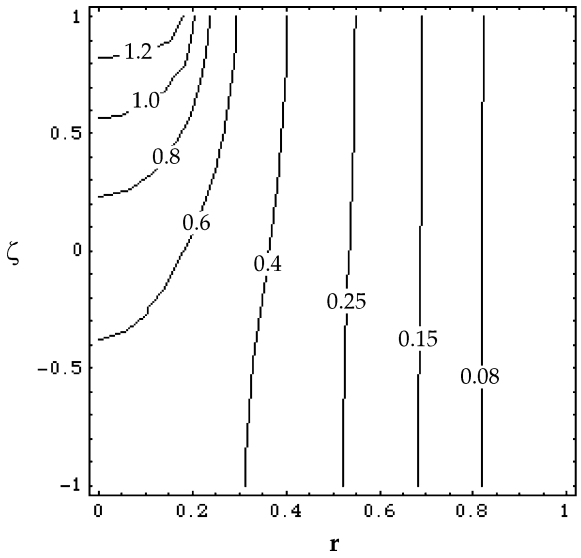

Fig. 2 Contours of the electric potential in the melt $\phi(r, \zeta)$ for $\gamma_e = 0.1905$ and $b = 0.4$.

radially outward and axially downward, as reflected in the contours of the electric potential, which are presented in Fig. 2 for $\gamma_e = 0.1905$ and $b = 0.4$, for which $\Phi_0 = 1.353$.

In a frame of reference moving with the fused-silica heater and crystal–melt interface, the melt motion is steady state. With the Boussinesq approximation, the equations governing the steady, axisymmetric melt velocity and temperature are

$$(\boldsymbol{v} \cdot \nabla)\boldsymbol{v} = -\nabla p + \alpha T \hat{\boldsymbol{z}} + \frac{\partial \phi}{\partial r}\hat{\theta} + Re^{-1}\nabla^2 \boldsymbol{v} \tag{7a}$$

$$\nabla \cdot \boldsymbol{v} = 0 \tag{7b}$$

$$Pr\,Re\left[\frac{\partial \boldsymbol{v}}{\partial t} + (\boldsymbol{v} \cdot \nabla)T\right] = \nabla^2 T + \Gamma \boldsymbol{j}^2 \tag{7c}$$

where p is the deviation of the dimensional pressure from the hydrostatic pressure for a uniform density normalized by $\rho_0 U_c^2$, and T is the deviation of the dimensional temperature from the melting temperature T_m normalized by $(T_h - T_m)$. In Eq. (7a), the ratio of the buoyancy force to the electromagnetic body force is $\alpha = \rho_0 g \beta (T_h - T_m)/J_c B$, which we refer to as the EM buoyancy parameter. Here, $g = 9.81$ m^2/s and β is the thermal volumetric-expansion coefficient. In Eq. (7c), the Prandtl number is $Pr = \mu c_p/k$, whereas the Reynolds number is $Re = \rho_0 U_c R/\mu$, where μ, c_p, and k are the dynamic viscosity, specific heat, and thermal conductivity of the melt, respectively. The Reynolds number is related to the strength of the electromagnetic stirring; that is, Re is directly proportional to $(BI)^{1/2}$. Here, the characteristic ratio of Joule heating to conductive heat transfer is $\Gamma = R^2 J_c^2/\sigma k(T_h - T_c)$. For the present process, $\Gamma = 7.4 \times 10^{-5}$, so that Joule heating is negligible.

In a frame of reference moving with the heater and the crystal–melt interface, the no-slip and no-penetration conditions on the surface of the outer electrode are

$$v_r = v_\theta = 0, \qquad \text{at} \qquad r = 1, \qquad \text{for} \qquad -1 \le \zeta \le +1 \tag{8a, 8b}$$

$$v_z = -\omega, \qquad \text{at} \qquad r = 1, \qquad \text{for} \qquad -1 \le \zeta \le +1 \tag{8c}$$

The boundary conditions on the crystal–melt interface and on the surfaces of the center electrode and fused-silica heater are

$$v_r = v_\theta = 0, \qquad \text{at} \qquad \zeta = -1, \qquad \text{for} \qquad 0 \le r \le 1 \tag{9a, 9b}$$

$$v_z = -\omega, \qquad \text{at} \qquad \zeta = -1, \qquad \text{for} \qquad 0 \le r \le 1 \tag{9c}$$

$$v_r = v_\theta = v_z = 0, \qquad \text{at} \qquad \zeta = +1, \qquad \text{for} \qquad 0 \le r \le \gamma_h \tag{9d, 9e, 9f}$$

Assuming that the density of the crystal and melt are the same, the gap between the heater and the outer electrode replenishes the solidifying melt at a volumetric flow rate $\pi\omega$, so that we assume a simple velocity profile

$$v_Z = \omega\left[-1 + \kappa_1(1 - r) + \kappa_2(1 - r^2)\right], \qquad \text{at} \qquad \zeta = +1 \qquad \text{for} \qquad \gamma_h \le r \le 1 \tag{10a}$$

where

$$\kappa_1 = \frac{3\left(1 + \gamma_h^2\right)}{(1 - \gamma_h)^3}, \qquad \kappa_2 = -\frac{2\left(1 + \gamma_h + \gamma_h^2\right)}{(1 - \gamma_h)^3(1 + \gamma_h)} \tag{10b, 10c}$$

which satisfies the no-slip and no-penetration conditions given by Eq. (9).

The thermal boundary conditions are

$$T = 0, \qquad \text{at} \qquad \zeta = -1, \qquad \text{for} \qquad 0 \le r \le 1 \tag{11a}$$

$$T = 1, \qquad \text{at} \qquad \zeta = +1, \qquad \text{for} \qquad 0 \le r \le 1 \tag{11b}$$

$$\frac{\partial T}{\partial r} = 0, \qquad \text{at} \qquad r = 1, \qquad \text{for} \qquad -1 \le \zeta \le +1 \tag{11c}$$

We have assumed that the rate of heat transfer from the outer electrode to the melt is small.

We introduce a Stokes stream function for the radial and axial velocities in the meridional circulations,

$$v_r = \frac{1}{r}\frac{\partial \psi}{\partial z}, \qquad v_z = -\frac{1}{r}\frac{\partial \psi}{\partial r} \tag{12a, 12b}$$

which identically satisfies conservation of mass for our axisymmetric melt motion. For given values of α, Pr, and Re, we solved for ψ, v_θ, and T using a Chebyshev spectral collocation method with Gauss–Lobatto collocation points in r and ζ. Since Eqs. (7a) and (7c) are nonlinear, we used a Newton–Raphson iterative method and incrementally increased Re from zero. After the Newton–Raphson method converged for a given Re, we used a continuation method to obtain initial guesses for the coefficients in the spectral representations for $(Re + \Delta Re)$. For each value of Re, the numbers of collocation points were varied to ensure that the results were independent of these number and to ensure that all boundary layers were adequately resolved. We used 75 collocation points in the radial direction and 46 collocation points in the axial direction.

III. Dopant Transport

Before solidification begins, the dopant concentration is uniform, and this initial value is used to normalize the concentration C, so that $C(r, \zeta, t = 0) = 1$. Once crystal growth starts, the dopant is rejected into the melt for $k_s < 1$, where k_s is the segregation coefficient, leaving a dopant-rich region near the crystal–melt interface. The flow convects the melt with the high Se concentration, thus referred to as "dopant-rich," away from the interface. The dimensionless equation governing this dilute species transport is

$$\frac{\partial C}{\partial t} + \boldsymbol{v} \cdot \nabla C = Pe_m^{-1}\nabla^2 C \tag{13}$$

where $Pe_m = U_c R/D$ is the species-transport Péclet number. Here D is the diffusion coefficient for the dopant in the molten semiconductor. Because the dopant concentrations are generally small, the dilute approximation is appropriate. We have assumed that the dopant density has no effect on the melt motion. In the future, we

will extend our models of solutal convection[8] during melt growth to treat solute transport during the present process.

The boundary condition for the crystal–melt interface is

$$\frac{2}{b}\frac{\partial C}{\partial \zeta} = Pe_g(k_s - 1)C, \qquad \text{at} \qquad \zeta = -1, \qquad \text{for} \qquad 0 \le r \le 1 \tag{14}$$

where $Pe_g = U_g R/D = \omega Pe_m$ is the growth Péclet number. The rejection of selenium into the melt at the crystal–melt interface due to solidification causes the concentration of the dopant in the melt to rise. In order to compensate for this elevated level of dopant, the melt is replenished with dopant-depleted melt, so that the boundary condition at the gap between the heater and the outer electrode is

$$C = k_s, \qquad \text{at} \qquad \zeta = +1, \qquad \text{for} \qquad \gamma_h \le r \le 1 \tag{15}$$

where $k_s = 0.1$ for gallium antimonide doped with selenium. The boundary conditions along the surfaces of the center electrode, outer electrode, and fused-silica heater are $\hat{\boldsymbol{n}} \cdot \nabla C = 0$.

Assuming that the dopant does not diffuse in the solid crystal and that the density of the solid and liquid are the same, the concentration in the crystal $C_s(r, z)$, normalized by the initial uniform dopant concentration in the melt, is given by

$$C_s(r, z) = k_s C(r, \zeta = -1, r = z/\omega) \tag{16}$$

The first-grown part of the crystal at $t = 0$ solidifies with $C_s(r, 0) = k_s$.

We use a Chebyshev spectral collocation method with a second-order implicit time integration scheme to solve Eq. (13) with 121 and 81 Gauss–Lobatto collocation points in r and ζ, respectively. We integrated from $t = 0$ to a t that is slightly less than h/ω, where h is the dimensionless length of the crystal, using 2000 time steps. We used a large enough number of time steps so that the results did not change when the number of time steps were increased.

IV. Results

We present results for $b = 0.4$, $\gamma_h = 0.8$, $\alpha = 4.449$, $Pr = 0.0443$ m/s, $U_g = 2$ mm/hr, and $U_c = 0.01027$ m/s, for which $\omega = 0.00005407$, $Re = 670.54$, and $Pe_m = 12,844$.

We present the contours of ψ, v_θ, and T in Figs. 3a, 3b, and 3c, respectively. In Fig. 3a, the meridional melt motion consists of two circulations in which upper circulation reflects melt motion in the counterclockwise direction adjacent to the heater and the lower circulation reflects melt motion in the clockwise direction adjacent to the crystal–melt interface. The melt flows radially inward adjacent to the crystal–melt interface. In Fig. 3a, the minimum and maximum values of ψ are -0.01266 and 0.01252, respectively. The electromagnetic body force in Eq. (7a) drives a negative azimuthal velocity, as reflected in Fig. 3b, where the minimum and maximum values of v_θ are -2.2061 and 0, respectively. In our estimation of the characteristic electric current density, we used a radial position $r_0 = 1$ cm. At this position, the magnitude of v_θ is approximately 1.86. For this azimuthal velocity, the electromagnetic body force is stirring the melt at 18 rpm. The isotherms in Fig. 3c reflect a small radial temperature gradient because the heat transfer is dominated by conduction. In Fig. 3c, the characteristic ratio of convective to conductive heat transfer, that is, the thermal Péclet number, is $Pe_t = PrRe = 29.71$.

Immediately after crystal growth begins, the rejection of selenium along the crystal–melt interface causes the concentration in the melt to rise above the initial uniform concentration $C = 1$. We present the constant-concentration curves in the melt when 0.05% of the crystal has grown at $t = 29.59$ in Fig. 4. In Fig. 4, the minimum and maximum values of the concentration are 0.1 and 1.016, respectively. The minimum value of the concentration for all stages of growth is 0.1 which is equal to the value of the segregation coefficient and which occurs at the gap for $\gamma_h < r < 1$ and $\zeta = +1$. The electromagnetic stirring causes strong convective mixing, as reflected in Fig. 4. For example, the $C = 0.95$ and $C = 1.0$ contours in Fig. 4 resemble the upper and lower circulations in the meridional

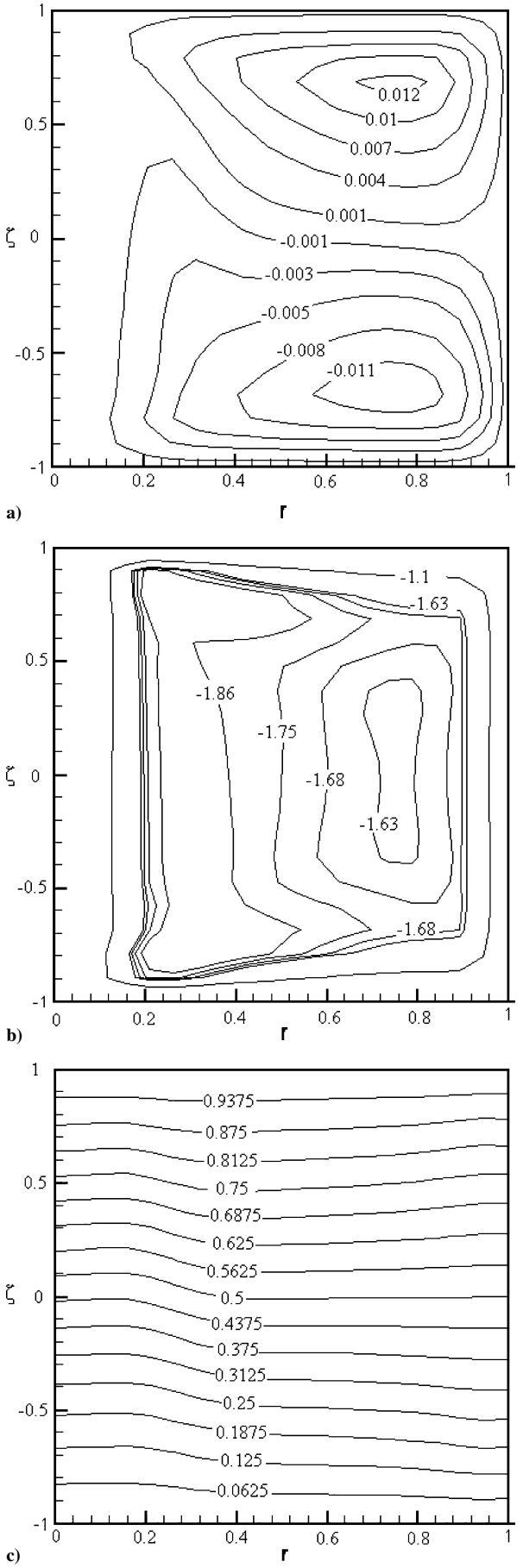

Fig. 3 Contours for the steady-state melt motion with $Re = 670.54$: a) meridional streamfunction $\psi(r, \zeta)$, b) azimuthal velocity $v_\theta(r, \zeta)$, and c) temperature $T(r, \zeta)$.

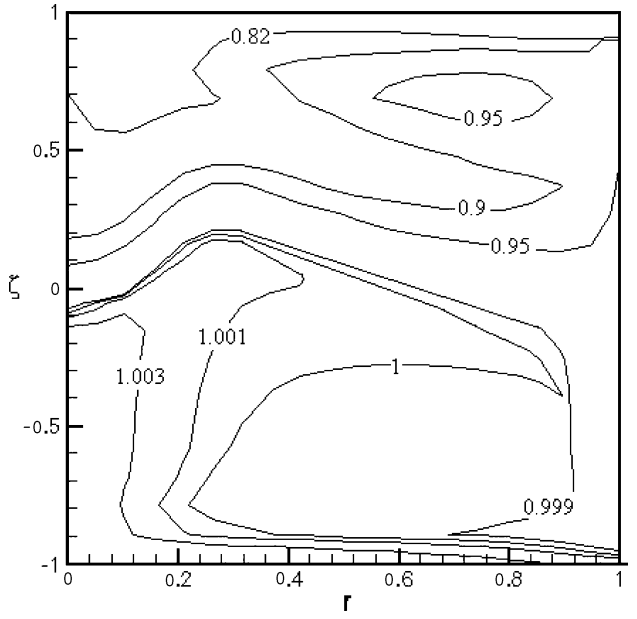

Fig. 4 Contours of the concentration in the melt $C(r, \zeta, t = 29.59)$ for unsteady dopant transport with $Re = 670.54$.

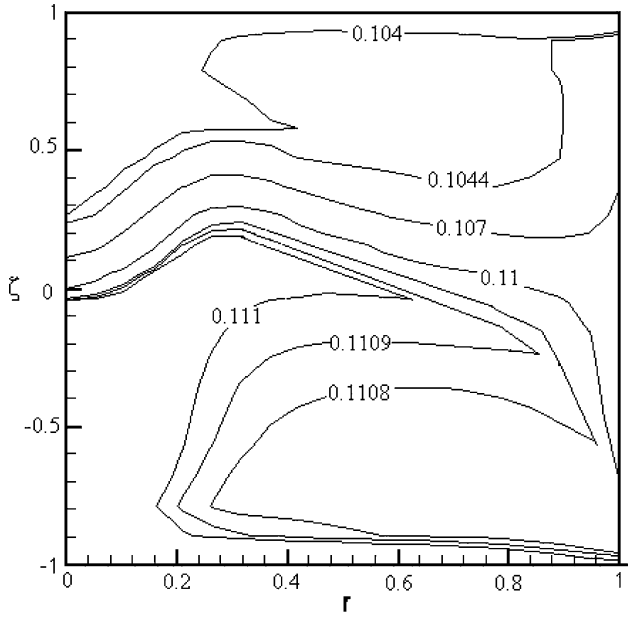

Fig. 5 Contours of the steady-state dopant concentration in the melt $C(r, \zeta, t = 10{,}000)$ with $Re = 670.54$.

melt motion presented in Fig. 3a. As growth progresses, the mixing causes the maximum value of the concentration in the melt to decrease. The strong convective mixing causes the dopant transport in the melt to reach steady state at a relatively early stage during growth. The initial transient is relatively short, occurring roughly at time $t = 10{,}000$, and the dopant transport is steady during most of the growth process. Once the dopant transport has reached steady state, the maximum value of the concentration in the melt has decreased to 0.1129, as shown in Fig. 5. For the present value of Pe_m, the convective species transport is much stronger than the diffusive species transport and the constant-concentration curves in Fig. 5 reflect a strong influence from the upper and lower circulations in the meridional melt motion in Fig. 3a.

For a dimensionless crystal length $h = 3.2$, the dimensionless time to grow the crystal is 59,183, and the dopant distribution in the crystal is presented in Fig. 6. In Fig. 6, there is very little radial segregation in the first-grown section of the crystal, which solidified during the early stages of growth corresponding to the times that the dopant transport is intrinsically unsteady. The remainder of the crystal which solidified after this initial transient exhibits an axially uniform dopant concentration, as reflected in the $C_s = 0.01118$, 0.01116, 0.01114, and 0.01112 contours in Fig. 6. The radial distribution of the dopant concentration in the crystal is presented in Fig. 7. The difference between the concentration at the centerline and at the periphery of the crystal is only $C = 0.00017006$. The electromagnetic stirring provides a strong convective dopant transport as reflected in the small variation of the concentration in the melt in Fig. 5, so that there is little radial segregation in the crystal.

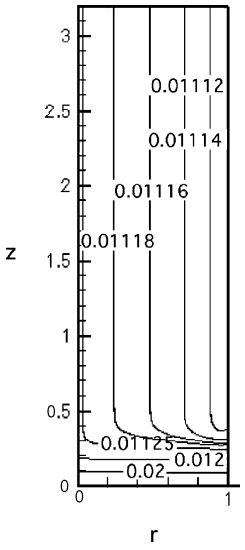

Fig. 6 Contours of the concentration in the crystal $C_s(r, z)$ with $Re = 670.54$.

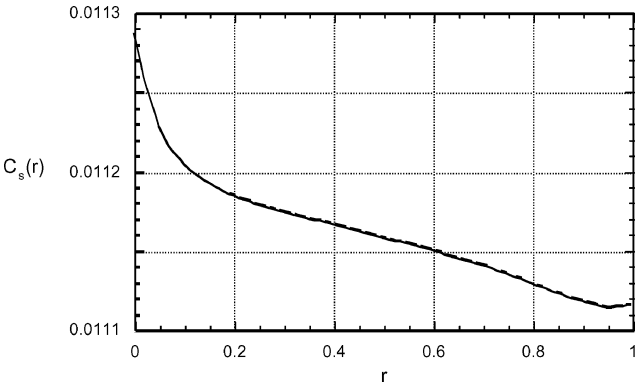

Fig. 7 Radial variation of the concentration in the crystal $C_s(r, z = 3.192)$ for steady-state dopant transport with $Re = 670.54$.

V. Conclusions

For vertical-gradient freezing using submerged heater growth and electromagnetic stirring, melt motion is instantaneously steady, whereas dopant transport is unsteady during the initial stages of growth. However, the electromagnetic stirring of the melt for Reynolds number $Re = 670.54$ causes relatively strong convective dopant transport, so that the dopant transport quickly reaches steady state and the remainder of the crystal solidifies with the same radial dopant distribution. The crystal has relatively little radial segregation. The configuration and parameters used in the present study were derived from real experiments. However, to date, characterization of the grown crystal in which electric density measurements are used to measure the dopant concentration are not complete. This characterization work is underway and will be investigated in a future study.

Acknowledgments

This research was supported by the U.S. Air Force Office of Scientific Research under grant FA9550-04-1-0249 and by the

NRC/USAF Office of Scientific Research Summer Faculty Fellowship Program. The calculations were performed on the Cray X1 provided by the DoD High Performance Computing Modernization Program under grant AFSNH2487 and on the IBM pSeries 690 provided by the National Computational Science Alliance.

References

[1]Morton, J. L., Ma, N., Bliss, D. F., and Bryant, G. G., "Dopant Segregation During Liquid-Encapsulated Czochralski Crystal Growth in a Steady Axial Magnetic Field," *Journal of Crystal Growth*, Vol. 242, No. 3/4, 2002, pp. 471–485.

[2]Ohmori, Y., Sugii, K., Akai, S., and Matsumoto, K., "LEC Growth of Te-Doped GaSb Single Crystals with Uniform Carrier Concentration Distribution," *Journal of Crystal Growth*, Vol. 60, No. 1, 1982, pp. 79–85.

[3]Ostrogorsky, A. G., "Numerical Simulation of Single Crystal Growth by Submerged Heater Method," *Journal of Crystal Growth*, Vol. 104, No. 2, 1990, pp. 233–238.

[4]Ma, N., and Walker, J. S., "A Model of Dopant Transport During Bridgman Crystal Growth with Magnetically Damped Buoyant Convection," *Journal of Heat Transfer*, Vol. 122, No. 1, 2000, pp. 159–164.

[5]Ma, N., Bliss, D. F., and Iseler, G. W., "Vertical Gradient Freezing of Doped Gallium–Antimonide Semiconductor Crystals Using Submerged Heater Growth and Electromagnetic Stirring," *Journal of Crystal Growth*, Vol. 259, No. 1/2, 2003, pp. 26–35.

[6]Glazov, V. M., *Liquid Semiconductors*, Plenum Press, New York, 1969.

[7]Jordan, A. S., "Estimated Thermal Diffusivity, Prandtl Number and Grashof Number of Molten GaAs, InP, and GaSb," *Journal of Crystal Growth*, Vol. 71, No. 3, 1985, pp. 551–558.

[8]Ma, N., "Solutal Convection During Growth of Alloyed Semiconductor Crystals in a Magnetic Field," *Journal of Crystal Growth*, Vol. 71, No. 3, 1985, pp. 551–558.